Received: 23 March 2024 | Revised: 25 July 2024 | Accepted: 28 August 2024

DOI: 10.1002/mp.17408

RESEARCH ARTICLE

MEDICAL PHYSICS

Experimental validation of a FLUKA Monte Carlo simulation for carbon-ion radiotherapy monitoring via secondary ion tracking

Pamela Ochoa-Parra[1,2,3] | **Luisa Schweins**[1,2,3] | **Nelly Abbani**[1,3,4] | **Laura Ghesquière-Diérickx**[1,2,5] | **Tim Gehrke**[1,3,6] | **Jan Jakubek**[7] | **Lukas Marek**[7] | **Carlos Granja**[7] | **Fabian Dinkel**[1,3] | **Gernot Echner**[1,3] | **Marcus Winter**[8] | **Andrea Mairani**[8] | **Semi Harrabi**[9] | **Oliver Jäkel**[1,3,8,6] | **Jürgen Debus**[8,9,6,10] | **Mária Martišíková**[1,3,6] | **Laurent Kelleter**[1,3,6]

[1]Heidelberg Institute for Radiation Oncology HIRO, National Center for Radiation Research in Oncology NCRO, Heidelberg, Germany

[2]Department of Physics and Astronomy, Heidelberg University, Heidelberg, Germany

[3]Department of Medical Physics in Radiation Oncology, German Cancer Research Center DKFZ, Heidelberg, Germany

[4]Medical Faculty Mannheim, Heidelberg University, Mannheim, Germany

[5]Medical Faculty, Heidelberg University, Heidelberg, Germany

[6]National Center for Tumor Diseases (NCT), NCT Heidelberg, a partnership between DKFZ and University Medical Center Heidelberg, Heidelberg, Germany

[7]ADVACAM s.r.o., Prague, Czech Republic

[8]Heidelberg Ion Beam Therapy Center (HIT), Heidelberg, Germany

[9]Department of Radiation Oncology, Heidelberg University Hospital, Heidelberg, Germany

[10]Clinical Cooperation Unit Radiation Oncology, German Cancer Research Center DKFZ, Heidelberg, Germany

Correspondence
Pamela Ochoa-Parra, Heidelberg Institute for Radiation Oncology, National Center for Radiation Research in Oncology NCRO, Heidelberg, Germany.
Email: pamela.ochoa@dkfz-heidelberg.de

Pamela Ochoa-Parra and Luisa Schweins share first authorship.

Mária Martišíková and Laurent Kelleter share last authorship.

Funding information
Deutsche Forschungsgemeinschaft, Grant/Award Number: 426970603; Nationales Centrum für Tumorerkrankungen Heidelberg

Abstract

Background: In-vivo monitoring methods of carbon ion radiotherapy (CIRT) includes explorations of nuclear reaction products generated by carbon-ion beams interacting with patient tissues. Our research group focuses on in-vivo monitoring of CIRT using silicon pixel detectors. Currently, we are conducting a prospective clinical trial as part of the In-Vivo Monitoring project (InViMo) at the Heidelberg Ion Beam Therapy Center (HIT) in Germany. We are using an innovative, in-house developed, non-contact fragment tracking system with seven mini-trackers based on the Timepix3 technology developed at CERN.

Purpose: This article focuses on the implementation of the mini-tracker in Monte Carlo (MC) based on FLUKA simulations to monitor secondary charged nuclear fragments in CIRT. The main objective is to systematically evaluate the simulation accuracy for the InViMo project.

Methods: The implementation involved integrating the mini-tracker geometry and the scoring mechanism into the FLUKA MC simulation, utilizing the finely tuned HIT beam line. The systematic investigation included varying mini-tracker angles (from 15° to 45° in 5° steps) during the irradiation of a head-sized

phantom with therapeutic carbon-ion pencil beams. To evaluate our implemented FLUKA framework, a comparison was made between the experimental data and data obtained from MC simulations. To ensure the fidelity of our comparison, experiments were performed at the HIT using the parameters and setup established in the simulations.

Results: Our research demonstrates high accuracy in reproducing characteristic behaviors and dependencies of the monitoring method in terms of fragment distributions in the mini-tracker, track angles, emission profiles, and fragment numbers. Discrepancies in the number of detected fragments between the experimental data and the data obtained from MC simulations are less than 4% for the angles of interest in the InViMo detection system.

Conclusions: Our study confirms the potential of our simulation framework to investigate the performance of monitoring inter-fractional anatomical changes in patients undergoing CIRT using secondary nuclear charged fragments escaping from the irradiated patient.

KEYWORDS

carbon-ion radiotherapy, charged nuclear fragments, in-vivo monitoring, Monte Carlo simulations, Timepix3

1 | INTRODUCTION

Monte Carlo (MC) simulations are widely recognized as the most accurate and powerful tools for modeling particle-tissue interactions in carbon ion radiotherapy (CIRT) and serve a variety of critical purposes ranging from treatment planning, dose verification, biological effects studies to treatment monitoring. The latter is of particular importance due to the pronounced dose gradient of carbon ions.[1] In CIRT, even minor changes in patient anatomy between treatment fractions, such as variations in tumor size, weight, or tissue swelling, can cause significant discrepancies between the planned and delivered dose distributions and ultimately affect treatment outcomes.[2,3]

Various CIRT monitoring methods have been proposed, mainly based on the detection of nuclear reaction products generated during the interaction of the carbon-ion beam with the patient's tissue.[4] Our research group at the German cancer research center (DKFZ, Heidelberg, Germany) has developed a monitoring method by tracking nuclear charged fragments using semiconductor silicon pixel detectors.[5]

Semiconductor pixel detectors are known for their effectiveness in radiation detection, characterized by their high time resolution. Among these, semiconductor silicon layers with Timepix3 readout chip detectors, developed by the Medipix collaboration at CERN (Geneva, Switzerland), known as Timepix3 detectors, have demonstrated their versatility in a range of applications within medical physics, particularly in the fields of medical imaging[6] and dosimetry.[7,8]

In recent preclinical studies conducted by our team, we used a configuration where two one-chip Timepix3 silicon pixel detectors were arranged one behind the other, resembling a mini-tracker. These studies covered various aspects such as monitoring the lateral positions of the pencil beams,[9] optimizing the positioning angles of the detectors for longitudinal beam monitoring,[10] assessing the influence of patient inhomogeneities,[11] and determining the detectability limits of air cavities within head-sized phantoms.

For the purpose of conducting a clinical trial, our research team developed a tracking system utilizing seven 4-chip Timepix3 mini-trackers.[12,13] These mini-trackers consist of a front and back layer, each with two chips placed side by side. This unique configuration was specifically assembled for the clinical trial's tracking system.[14] The In-Vivo Monitoring (InViMo) prospective clinical trial is dedicated to monitoring patients with head and neck tumors, as well as central nervous system (CNS) tumors, undergoing CIRT treatments at the Heidelberg Ion Beam Therapy Center (HIT, Heidelberg, Germany).

The goal of this work was to systematically validate, for the first time, the implementation of the Timepix3-based mini-tracker used in the InViMo tracking system in (MC) simulations for monitoring secondary charged fragments in CIRT. Comparisons between experimental data and MC simulations were conducted with a focus on studying the variables crucial for our monitoring method.

We utilized the FLUKA general-purpose MC code,[15,16] renowed for its strong focus on medical applications.[16,17] FLUKA has undergone extensive development and validation for medical applications, particularly for ion radiotherapy.[18–20] FLUKA's robustness has been demonstrated through thorough benchmarking against depth-dose data and lateral-dose profiles from various ion-beam therapy and research facilities.[21–23] Furthermore, FLUKA has been selected by a commercial vendor for validation purposes and to

provide physics input data for their newly developed carbon-ion module.[24] It was also used to validate a fast MC dose engine for CIRT.[25] Additionally, hadronic interactions in FLUKA have been thoroughly benchmarked against experimental data.[16,26–28] For instance, the total reaction cross-sections for carbon ions interacting with hydrogen, carbon, and oxygen were benchmarked against experimental data from multiple sources.[29–34] Comparison of fragment yields at different depths in water was performed based on these measurements, as well as with experimental data[35] involving carbon ions at 400 MeV/u impacting a thick water target.

As FLUKA serves as a gold standard tool in hadron therapy, a dedicated in-house FLUKA MC framework was developed at HIT providing automated simulations for clinical treatment plans delivered by actively scanned proton, carbon,[36,37] and helium-ion beams.[38] Since the InViMo clinical trial and associated experiments of this work are conducted at HIT, the modeled beam line of the FLUKA MC framework of HIT was used to ensure realistic reproduction of the real-world scenario for the delivery of CIRT treatment.

In the Materials and Methods, we outline the HIT beam line, experimental setup, mini-tracker, and FLUKA MC simulation. Section 3 compares experimental data with MC simulation results for fragment distributions, track angles, emission profiles, and detected fragment counts. Section 4 interprets the findings, considering measurement uncertainties and detection significance. Finally, Section 5 summarizes outcomes and discusses implications for the InViMo monitoring project.

2 | MATERIALS AND METHODS

2.1 | Experiment

2.1.1 | Heidelberg Ion Beam Therapy Center

The experiments were conducted at the HIT in Heidelberg, Germany. HIT is a hospital-based facility that specializes in ion-based radiotherapy treatments, serving more than 1000 patients annually. HIT employs a synchrotron to accelerate four types of ions: protons, carbon, helium, and oxygen ions. Proton and carbon ions have been used for therapeutic purposes since 2009.[39]

The HIT facility comprises three treatment rooms and one experimental room. Two treatment rooms and the experimental room feature fixed horizontal beam lines, whereas the third treatment room has a 360° revolving gantry. In the dedicated experimental room at HIT, measurements were performed to validate the FLUKA MC implementation of the Timepix3-based mini-tracker response to secondary ions during carbon-ion treatment. The InViMo clinical trial takes place in a treatment room with a horizontal beam.

HIT utilizes the intensity-modulated raster-scanning technique for irradiating tumors.[40] In this technique, the beam is scanned across the tumor in a raster pattern, and the energy of the beam is modulated to conform to the specific shape and depth of the tumor. To ensure uniform dose distribution within the tumor and minimize the impact on healthy tissue, a ripple filter is employed, allowing for further refinement of the ion energy spread.

For carbon ions, 255 discrete beam energies are available, spanning from 88.83 to 430.00 MeV/u, corresponding to penetration depths ranging from 2 to 30 cm in water. The clinical intensity of carbon-ion beams ranges from 10^6 to 10^{10} ions/s. The monitoring of the ion-beam intensity and position is facilitated by the beam application and monitoring system (BAMS), situated within the beam nozzle.

2.1.2 | Mini-tracker

We employed a customized configuration of Timepix3 detectors called AdvaPIX TPX3 Quad (quad module)[12,13] developed at ADVACAM s.r.o. (Prague, Czech Republic). It resembles a mini-tracker with two layers - front and back - as is illustrated in Figure 1. Each layer consists of two Timepix3 chips. The two sensitive layers in the mini-tracker are separated by a distance of 20.3 mm.

The seven mini-trackers incorporated into the detector system for the InViMo trial have a sensitive layer thickness of 300 μm, whereas the one used in this work uses a 500 μm-thick silicon sensor. Aside from these differences in sensitive layer thickness, all components in the detectable region of our (AdvaPIX TPX3 Quad) modules are identical.

Within each layer, the two Timepix3 chips share a continuous sensitive silicon sensor with a surface area of approximately $14 \times 28\,\text{mm}^2$. For the detector used in our work, the sensitive layer thickness is 500 μm. This silicon sensitive layer is bump-bonded to two Timepix3 readout chips. The pixel size is $55 \times 110\,\mu\text{m}^2$ around the TPX3 chip edges, $110 \times 110\,\mu\text{m}^2$ in the chip corners, and $55 \times 55\,\mu\text{m}^2$ everywhere else. Two columns of bump bonds must be omitted for technical reasons at the intersection zone of the two Timepix3 chips. Consequently, this leads to two pixel columns effectively doubling in pixel size in the intersection zone in the middle of the sensitive layer.

The mini-tracker offers a remarkable time-binning resolution of 1.56 ns. Each radiation-sensitive pixel records data about the timing, energy, and impact positions of incoming ions. Data readout is performed via USB3.0. The mini-tracker experiences no dead time as long as the data throughput does not exceed 47 million pixels/s. We have designed the experiment to ensure that the data rate does not exceed 5 million pixels/s, thus ensuring negligible dead time during measurements. In order

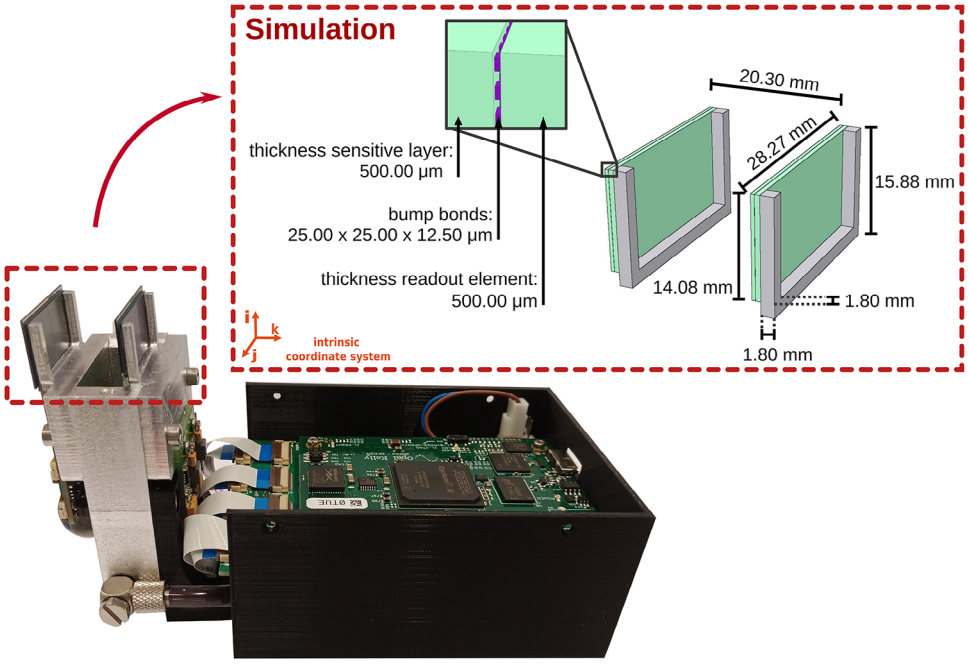

FIGURE 1 Implementation of the mini-tracker in the FLUKA simulation. At the bottom of the image, there is a picture of the mini-tracker. The sensitive region of the detector implemented in the FLUKA MC simulation is shown in the red dashed box. The sensitive region in FLUKA MC comprises the silicon sensitive layer, the bump bonds, the readout, and the U-shaped aluminum bars.

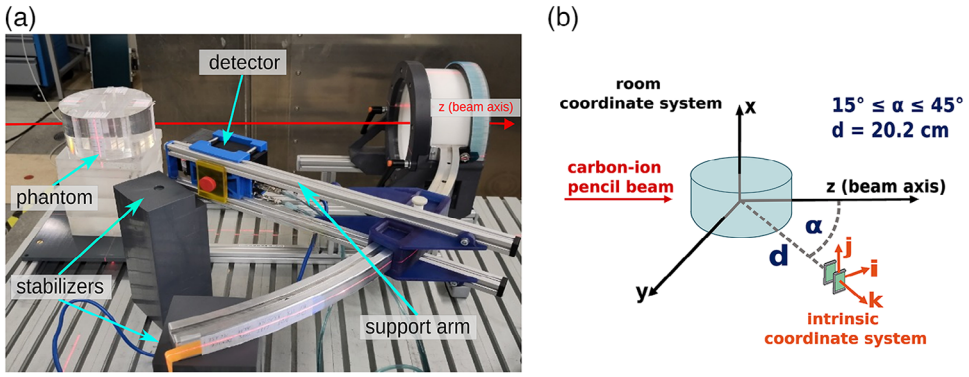

FIGURE 2 Experimental setup. (a) Photograph of the measurement setup in the experimental room at HIT. (b) Schematic of the measurement setup, showing both the room coordinate system and the intrinsic (detector) coordinate system. The detector positioning angles are represented by α. Measures and proportions are not to scale.

to achieve noise-free data acquisition, we set a minimum energy threshold per pixel of 3 keV.

2.1.3 | Experimental setup

In this experiment, we used a custom mini-tracker support setup developed in-house, as illustrated in Figure 2a, which has an aperture for the beam. As a head model, a homogeneous PMMA (PolyMetyl-MethAcrylate) phantom with a diameter of 16 cm was positioned in the isocenter of the experimental room. The setup includes a straight aluminum rail that supports the mini-tracker. Along this rail, the distance of the mini-tracker to the isocenter can be adjusted. Additionally, an arc-shaped aluminum bar, on which the aluminum rail can slide, allows for a convenient positioning of the detector relative to the beam axis. Figure 2b shows the position of the mini-tracker within the support setup. The detector, rotated 90° around its intrinsic k-axis, is held by the support arm. The sensitive layers of the mini-tracker had a forward-leaning tilt of 1.65° around the intrinsic j-axis towards the beam axis. The distance between the mini-tracker and the room isocenter is 20.2 cm, which is the average distance used in the InViMo detection system. To systematically investigate the mini-tracker's response at various angles α, the mini-tracker was positioned at 15° to 45° relative to the beam axis in steps of 5°.

A total of seven irradiation plans were developed, one for each mini-tracker position. All plans used 10 therapeutic pencil beam energies covering a 5 cm-long target

TABLE 1 Used pencil-beam parameters.

Parameter	Minimum	Maximum
Total number of primary carbon-ions	4.7×10^8	78.4×10^8
Pencil-beam intensity	2×10^6 ions/s	20×10^6 ions/s
Pencil-beam focus (FWHM)	6.1 mm	7.5 mm
Pencil-beam energy	160 MeV n^{-1}	255 MeV n^{-1}

Abbreviation: FWHM, full width at half maximum.

region around the isocentre. For all energies, the position of the pencil beam was set constant in the centre of the lateral plane (x = y = 0). The number of primary carbon ions was selected based on both pencil beam energy and mini-tracker position to achieve an average detection of approximately 1×10^6 fragments per mini-tracker position. In addition, the intensity of each pencil beam was carefully adjusted to optimize the measurement time while avoiding data rate overload on the mini-tracker. Table 1 outlines the parameter ranges employed in the irradiation plans.

2.2 | MC simulations

2.2.1 | FLUKA

In this study, the simulations were performed using the fully integrated particle physics MC simulation package FLUKA,[15,16] (version 2021.2.5), known for being an extensively benchmarked simulation tool for particle therapy. We used the HADROTHE package with default settings tailored for ion therapy.

FLUKA's nuclear interactions are described by the PEANUT (Pre-Equilibrium Approach to NUclear Theramilzation) model,[41,42] which employs a generalized intranuclear cascade, pre-equilibrium particle emission, an equilibrium phase, and statistical techniques for nucleon evaporation, fragmentation, and γ-ray emission.[16,41,43] FLUKA uses the Boltzmann Master Equation (BME) theoretical approach to describe the nuclear thermalization of heavy ions at low energy ranges up to 150 MeV/u.[44,45] FLUKA utilizes the modified RQMD-2.4 (Relativistic Quantum Molecular Dynamics) model for ion reactions in the GeV/n energy range down to $\approx$ 0.1 GeV/n. It processes excited fragments from RQMD using the PEANUT model. Notably, the most recent FLUKA update included new physics models for coherent and quasi-elastic scattering of hadrons on nuclei, and revised cross-sections for interactions between protons and light ions.[46]

The multiple scattering formalism for the transport of charged particles through matter implemented in FLUKA, based on the Molière theory, was developed specifically for FLUKA, as described in ref. [47].

To enhance the precision of simulating the generation of light fragments such as protons and alpha particles, which are critical for an accurate representation of secondary fragment production,[18] we activated the evaporation, and coalescence physical models. To optimize computational efficiency, we deactivated delta rays and set an energy threshold of 20 MeV for low-energy neutron interactions. Since they mainly deposit energy locally in the tissue, they would not significantly impact the detector's detection of charged nuclear fragments escaping from the irradiated patient.

Two FLUKA MC user routines were modified to further customize the simulation: source.f used to define the source of particles in a simulation and mgdraw.f for scoring fragments with the implemented mini-tracker.

2.2.2 | Implementation of the mini-tracker in the FLUKA MC

To reproduce our CIRT monitoring method accurately, we integrated the geometry of the mini-tracker structure and fragment detection mechanism into the FLUKA MC simulation.

From the geometry aspect, we have replicated all the elements within the sensitive region of the mini-tracker, as illustrated in Figure 1. Those components are the sensitive silicon layers, the bump bonds connecting it to the readout chip, and the aluminum bars that support the sensitive parts of the mini-tracker. Both the sensitive layer and the readout chip were implemented as plates of solid silicon. The silicon thickness of the sensitive layer and the readout chip is 500 μm each. The 256 $\times$ 512 bump bonds are modeled as cuboids of 25 μm.[48] The material composition of the bump bonds was implemented as a mixture of 63% tin and 37% lead, closely resembling the actual material composition. The metallic U-shaped bars are composed of aluminium. As explained in section 2.1.2, for technical reasons there is a 110 μm-wide gap between the two Timepix3 chips without bomb bonds.

The mgdraw.f user routine has been customized to identify charged particles passing through the mini-tracker based on a specific criterion: the particle must deposit energy greater than the defined detection threshold in both sensitive layers of the mini-tracker, which, in our measurement, is set at 3 keV. When this criterion is met, several attributes of the particle are recorded, including its spatial entry coordinates, particle type, kinetic energy, and energy loss in both sensitive layers, among others.

2.2.3 | HIT beam line and treatment plan delivery

We utilized the experimentally verified model of the HIT beam line as described in refs. [21, 23]. In contrast to employing the default sampling procedure as defined in the FLUKA source.f user routine, we opted to customize it to ensure the delivery of all primary carbon-ion

particles from the generated irradiation plans. As mentioned in Section 2.1.2, the seven irradiation plans were created including the same pencil-beam energies but different amounts of carbon ions per pencil beam depending on the mini-tracker position. These irradiation plans were composed as plain text documents and interpreted by the source.f routine.

2.3 | Data post-processing

As described in Section 2.2.2, in the simulation, the two coincident hits of a fragment in the mini-tracker are inherently correlated, enabling their direct use in determining the fragment track.

In the measurement, the raw data must first be pre-processed before the fragment track can be reconstructed. For this purpose, an in-house written Matlab routine (Matlab version 2021b) was used.

In the data-processing pipeline, clusters are formed by grouping pixel signals from neighboring pixels, including diagonal neighbors. A cluster is established when the maximum timestamp difference among its constituent pixels is 500 ns to ensure completeness of clusters. A cluster timestamp is defined as the earliest timestamp among these pixels. The position of the particle impact is determined by calculating the center of the cluster, utilizing the energy-deposition-weighted mean of the pixel coordinates within the cluster.

After building the clusters from the measured data, the independent clusters in the two sensitive layers need to be matched. Coincident clusters with a timestamp difference of 75 ns are considered to belong to a single fragment track in order to account for potential timestamping and synchronization errors. In cases where multiple clusters exist within this coincidence window, those with the smallest time difference are associated to the same fragment.[13] To enable the reconstruction of fragment tracks in the treatment room, these clusters are transformed into the room coordinate system using the known position of the mini-tracker.

In both the simulation and the measurement, a reconstructed fragmentation vertex (fragment origin) is defined as the midpoint along the shortest connection line between the back-projected fragment track and the pencil-beam path line.[11]

2.4 | Validation of simulation accuracy

To assess the accuracy and reliability of our FLUKA MC simulation in monitoring carbon-ion treatments with charged nuclear fragments, we conducted a comparative analysis between the experimental results and our simulation outputs. This comparison focuses on five key parameters.

First, we explored the distribution of crosspoints of fragment tracks across the front sensitive layer of the mini-tracker. Second, we performed an analysis of detected fragment tracks to evaluate how well the simulation replicates phenomena such as fragment production, scattering and absorption. Third, we studied reconstructed fragment emission profiles, which are used by our group for the identification and localization of internal geometrical changes along the beam axis.[9–11] Fourth, we performed an analysis of the number of detected fragments as a function of the position of the mini-tracker and, fifth, as a function of the pencil-beam energies.

For the first three parameters, the comparative analysis was conducted with data from the detector positioned at $\alpha = 30°$ since it represents the midpoint of the studied angle range. Regarding the number of detected fragments as a function of the mini-tracker's position and the pencil-beam energy, we compared the measured data and data obtained from the MC simulations from the seven mini-tracker positions.

3 | RESULTS

3.1 | Distribution of detected fragments across the detector surface

The comparison between the detected fragment tracks in measurement and simulation demonstrates a good qualitative resemblance. Figures 3 display the 2D distribution of crosspoints of fragment tracks with the front sensitive layer for both the measured data and data obtained from the simulations, respectively, with the detector positioned at $\alpha = 30°$. Additional projections along the respective axes provide a more comprehensive perspective.

A distinctive feature is evident in the j-axis histograms (top projections), characterized by a peak spanning two pixels at j-pixel coordinates 256 and 257. This phenomenon is attributed to the absence of bump bonds in two columns, one per chip's edge, within the zone between the two Timepix3 chips (see Section 2.1.2). In the measurement, this results in an effectively doubled pixel size for these columns. To replicate this in the simulation during data post-processing, fragments striking the one-pixel-wide edge row per chip are assigned to the nearest pixel (j-pixel 256 for the left chip and 257 for the right chip). The outcome is depicted in Figure 3b, where the peaks in both images rise with the same magnitude.

Since our monitoring method relies on the evaluation of fragment tracks, fragments that cross only one detector layer are not taken into account in either the measurement or the simulation. Hence, there is a decreased chance of detecting fragments near the edges of the sensitive layers. This effect is seen in Figure 3, where a reduction in the number of fragment tracks is observed towards the left, right, and upper edges, given the 90° intrinsic rotation of the detector in

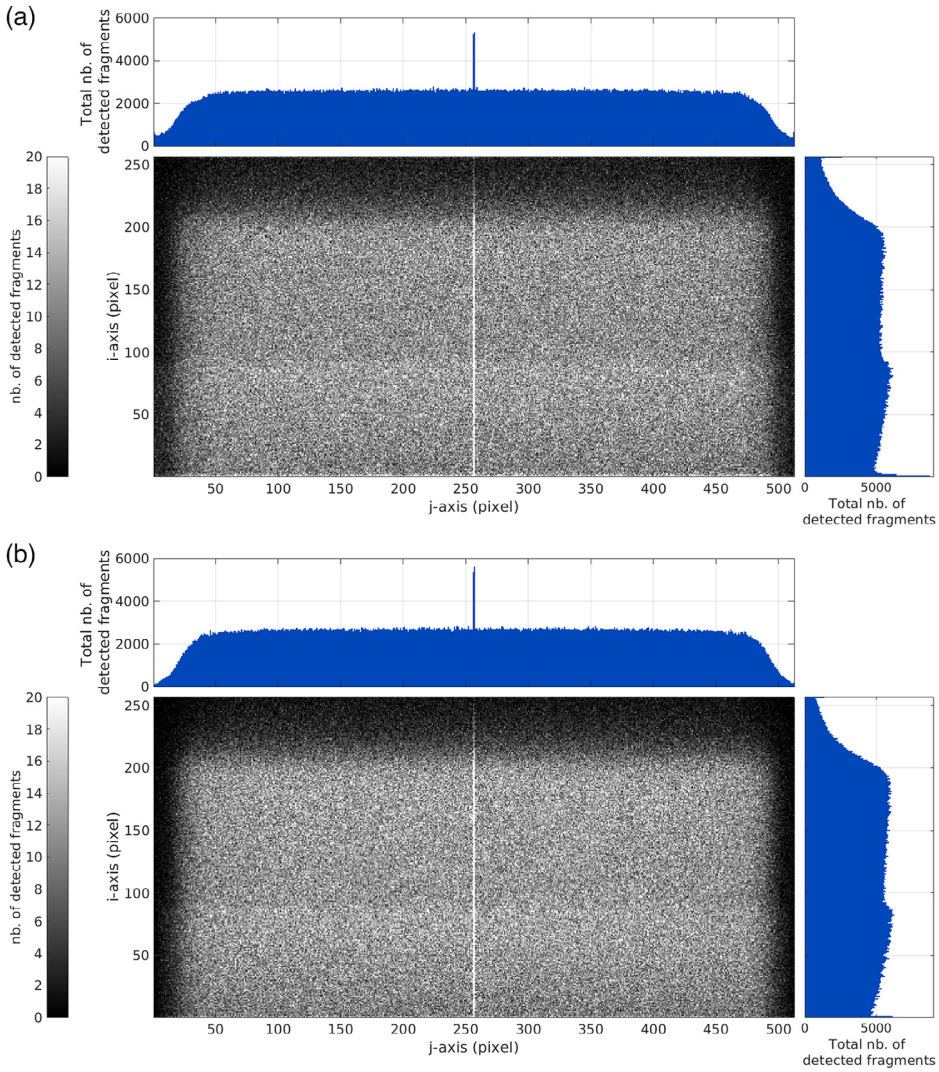

FIGURE 3 Number of detected fragment tracks across the front sensitive layer with integrated number of fragments along the columns or rows. Detector position: $\alpha = 30°$ relative to the beam axis. (a) Measurement. (b) Simulation.

the experiment and thus in the simulation as is shown in Figure 2b. In both the measurement (figure 3a) and simulation (Figure 3b), we consistently observed a proportional reduction in the number of fragment tracks in these regions. A local maximum is observed in the lower third of the i-axis histograms (right projections) that corresponds to fragments generated in the beam nozzle about 108 cm upstream of the isocenter. Since the fragment emission is strongly forward-peaked, there is an effective cut-off at an i-axis value of 100 in the front layer, beyond which fragments from the beam nozzle will miss the back detector layer.

3.2 | Angular distribution of detected fragment tracks

In Figure 4, the angular distributions between the fragment tracks and the beam axis α_z are illustrated.

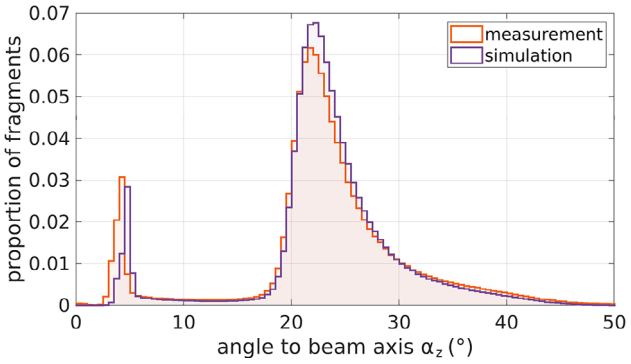

FIGURE 4 Histogram of the angles between the detected fragment tracks and the beam axis (α_z) for the detector positioned at $\alpha = 30°$.

The number of fragment tracks, normalized to the number of primary carbon ions irradiated, shows quantitative agreement between the measurement and the

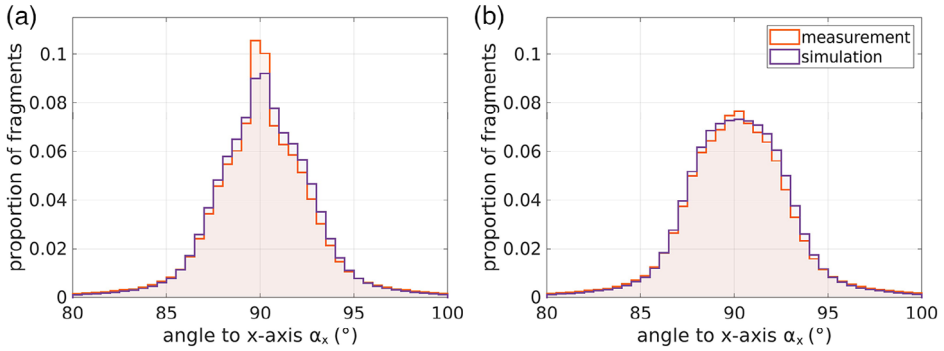

FIGURE 5 Distribution of the angles between the fragment tracks and the vertical room-coordinate x-axis. (a) All fragments. (b) Excluding fragments from the beam nozzle ($\alpha_z < 12^\circ$).

simulation, with an integrated difference of only 0.5%. Two prominent peaks are observed in the histogram. The first peak represents fragments generated in the beam nozzle at angles ranging from 3° to 6° relative to the beam axis. Notably, there is a slight rightward shift in the simulation peak. We quantified the shift by calculating the mean value in the region of interest, between 2° and 8°. For the measurement peak, the mean value is $4.1 \pm 0.2^\circ$, while for the simulated one, it is $4.6 \pm 0.1^\circ$. Additionally, the simulated peak contains about 30% less fragment tracks compared to the measurement.

The second peak corresponds to fragments that originate in the phantom, which exhibit track angles to the beam axis that exceed $\alpha_z = 12^\circ$. In this peak, less fragments are observed in the measurements compared to those observed in the simulation. The median angles between the fragment tracks and the beam axis in the region of $\alpha_z > 12^\circ$ are $\text{med}(\alpha_z)_m = 25.0 \pm 0.1^\circ$ for measurement and $\text{med}(\alpha_z)_s = 24.8 \pm 0.1^\circ$ for simulation.

The angular distributions between fragment tracks and the vertical x-axis were also studied. Figure 5a illustrates the distribution of the fragment tracks along the x-axis α_x, showing symmetrical track angle distributions centered around $90.0 \pm 0.2^\circ$ in both our measurement and simulation results. The prominent peak in the plot is primarily due to fragments originating directly from the beam nozzle, which have track angles to the beam axis below 12°. When these fragments are excluded from the analysis, as shown in Figure 5b, the peak disappears. The distribution is characterized by consistent median track angles of $\text{med}(\alpha_x) = 90.2 \pm 0.2^\circ$ for both the measurement and simulation data sets, along with comparable full width at half maximum (FWHM) values of $(5.7 \pm 0.2)^\circ$ for the measurement and $(5.8 \pm 0.2)^\circ$ for the simulation.

3.3 | Reconstructed fragment emission profiles

Fragmentation emission profiles are histograms that illustrate the distribution of reconstructed fragmentation vertices along a specific axis coordinate. As mentioned in Section 2.3, we defined these vertices as the coordinates of the midpoint of the shortest connecting line between the back-projected fragment track and the pencil beam axis.

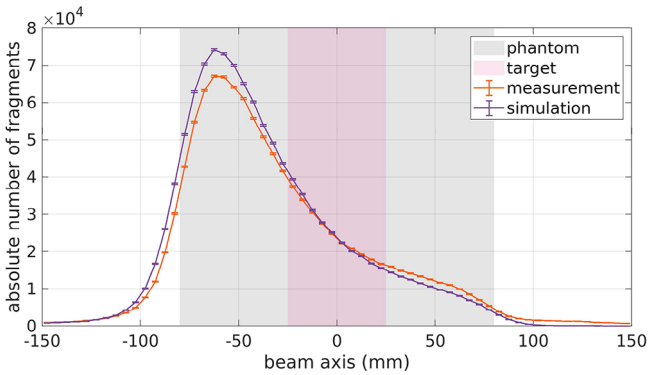

FIGURE 6 Simulated and measured fragment emission profiles along the beam direction with the detector positioned at $\alpha = 30^\circ$. The gray shadow indicates the position of a head-sized phantom, centered at the isocenter of the room, and the red shadow outlines the virtual target area.

The uncertainty of the number of reconstructed fragmentation vertices N_{rFV} is given by $\sigma(N_{\text{rFV}}) = \sqrt{N_{\text{rFV}}}$. Figure 6 shows the reconstructed fragment emission profiles from both measurement and simulation along the beam axis for the detector located at $\alpha = 30^\circ$. The beam comes from the negative direction, and the gray area in the figure indicates the position of the head-sized phantom centered at the room isocenter with its front surface at $z = -80$ mm. The red shadow represents the virtual target area.

The measured and simulated emission profiles have similar shapes. The simulated profile shows a slight shift of the rising edge to the left compared to the measured profile. The simulation indicates that there is a greater number of fragments in the entrance region of the phantom than what was observed in the measurement. Conversely, towards the end of the profile, at a depth of approximately 50 mm, a slightly higher number of fragments is observed in the measurement.

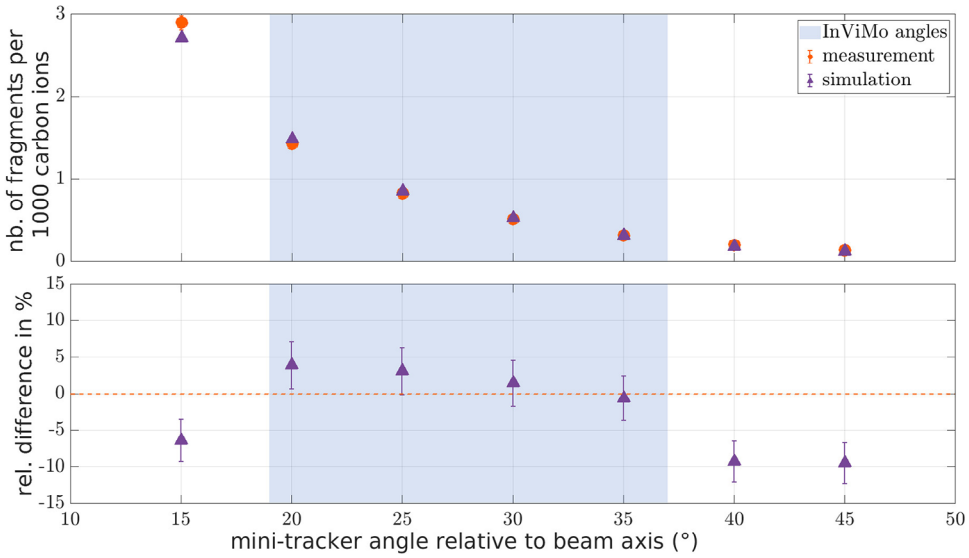

FIGURE 7 Number of fragments per 1000 primary carbon ions depending on the detector position. The light blue shadow represents the range of angles in which the detectors of the InViMo detection system are located. The top panel shows the number of detected fragments per primary carbon ion f. The lower panel shows the relative difference of the data obtained from the simulations compared to the measurement.

3.4 | Number of detected fragments depending on the detector position

The top panel of Figure 7 displays the absolute number of detected fragments per primary carbon ion f as a function of the detector position. Meanwhile, the bottom panel showcases the relative difference between the data obtained from the simulations and the data obtained from the measurements. The blue-shaded region of the plot represents the detector angles within the InViMo detection system.

The error bars represent the uncertainty σ_f in the number of detected fragments per carbon ion f. This uncertainty σ_f comprises two components: the uncertainty in the total number of detected fragments $\sigma_F = \sqrt{F}$ and the uncertainty in the number of delivered carbon ions σ_C. In the simulation, the uncertainty in the number of delivered carbon ions is zero, as we did not employ a sampling approach. Instead, we defined in the source.f user routine to simulate the exact number of planned carbon ions per irradiation plan. For the experiment, the uncertainty in the number of delivered carbon ions σ_C arises from the uncertainty in the calibration of the ionization chambers within the BAMS at HIT and is estimated to be at most 3%.

In both simulation and measurements, a consistent decrease in the number of detected fragments is observed as the angle increases. The relative difference between simulation and measurement in the number of fragments detected for the InViMo angles remains below 4%. The detector located outside of our region of interest, at 40° and 45°, exhibits differences below 10%.

3.5 | Number of detected fragments per pencil-beam energy

Figure 8 shows the number of fragments per primary carbon ions at different pencil beam energies. The data set used in this plot includes the data from all detector positions, $\alpha = (15, 45)°$. The top panel of the figure shows the absolute number of fragments detected per primary carbon ion, as a function of the 10 pencil beam energies included in the irradiation plan. The bottom panel shows the relative difference between the data obtained in the simulations and the measurements. As mentioned in 3.4, the uncertainties in the detected fragments per carbon ion (σ_f) come from the total number of fragments detected (F) and from the delivered carbon ions (C). The simulation has zero uncertainty in the delivered ions. In the experiment, σ_C is reported to be at most 3%. The number of detected fragments increases with increasing energy in both the experiment and the simulation. The simulation underestimates the production of fragments by less than 5% in all cases, with the largest discrepancies observed for lower and higher pencil-beam energies.

4 | DISCUSSION

Our findings show a consistent agreement between measurements and simulations, thus validating the implementation of the mini-tracker and the associated scoring method within our FLUKA simulation framework. When examining the distribution of detected fragments across the front-sensitive layer of the

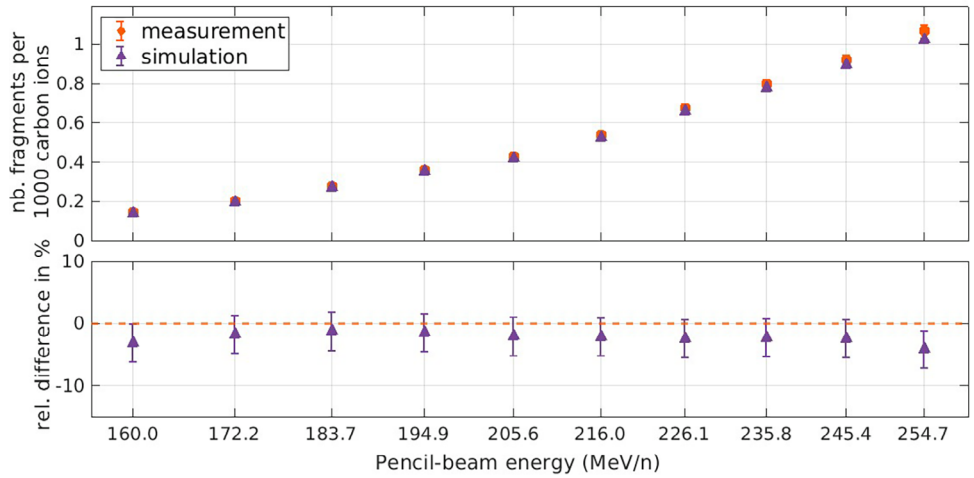

FIGURE 8 Number of fragments per 1000 primary carbon ions depending on the pencil-beam energy. The top panel shows the absolute number of detected fragments per primary carbon ion f. The lower panel shows the relative difference of the data obtained from the simulations compared to the measurement.

detector positioned at $\alpha = 30°$ with respect to the beam axis in Figure 3, all observed features exhibit remarkable similarity between measurements and simulation.

The angular distribution of fragments along the beam axis exhibits only a 0.5% difference between the measurement and the simulation, as shown in Figure 4. Agreement is particularly visible at the rising edge of the main peak in the angular distributions along the beam axis, which originates from phantom fragment tracks. From Figure 5b, the measured and simulated distributions of the track angles relative to the vertical room axis are in agreement within their uncertainties when fragments generated in the beam nozzle are not taken into account.

The similarities observed in the fragment track distributions between measurement and simulation also extend to the reconstructed emission profiles. As shown in Figure 6, the overall shape of the emission profiles is very similar, with differences of 2.0% in the number of fragments in the emission profile for the detector located at $\alpha = 30°$, and less than 4% for the detector positions in the region of interest of the InViMo detection system used.

For the number of fragments detected at all detector positions, as shown in Figure 7 we observed an exponential decrease in the measured fragment yield with increasing angle to the beam axis. This effect was also observed in our simulations, which reproduce a similar slope in the number of fragments detected as a function of the mini-tracker position, which is consistent with previously reported results by our group in the study investigating the appropriate detection angles for carbon ion radiotherapy monitoring.[10] In another study[49] that compares ion fragmentation measurements with simulations (Geant4 toolkit version 9.2), the analysis of detected proton yields as a function of the detection angle from 0 to 60° for a 200 MeV/u ^{12}C beam also showed an exponential decrease as the angle to the beam increased. However, the simulations consistently overestimated secondary proton yields, ranging from 10% to 40%.

As expected, the yield of detected fragments increases with the ion range (i.e., the pencil beam energy), as shown in Figure 8. This is attributed to the ions' ability to penetrate deeper into the head-sized PMMA phantom, engaging with a larger volume of material and consequently increasing the probability of interaction with the phantom. Differences of less than 5% in the number of detected fragments in the range of pencil-beam energies studied, from 160 to 255 MeV/n, confirm a consistent agreement between measurements and simulations. The FLUKA version used in this work (version 2021.2.5), and the Timepix3-based mini-tracker used in our monitoring project experiments demonstrate robustness. The discrepancies observed in our study are significantly smaller than those reported in the cited study,[49] which ranged from 10% to 40%, reinforcing the reliability of our implementation.

The remaining minor discrepancies between our measurements and the FLUKA MC simulations can be attributed to two primary sources. The first source is the MC code, FLUKA, itself. As mentioned in the Introduction, FLUKA is considered the gold standard for CIRT simulation, since its hadronic models appear to be adequate for physical dose calculations.[18,19] The theory of electromagnetic interactions is well established, and their integration into MC codes is a standardized process. In contrast, the same cannot be said for the nuclear interactions responsible for secondary production, as there are no rigorous calculable models available for an accurate description.[50]

In a previous publication by our group, they investigated carbon-ion fragmentation in water and PMMA targets.[51] Differences between the FLUKA simulation (version 2011.2c.0) and the measurements were found, highlighting the need for improvements in the nuclear models since then. Experimental data are necessary for benchmarking and allowing for such improvements due to the intrinsic phenomenological nature of the calculation models. FLUKA has undertaken benchmarking[27] to enhance its accuracy for tissue-like targets in the therapeutic energy range. This was based on experiments aimed at measuring total cross-sections in thin targets.[52–55] Despite significant advancements in physics models in recent decades, the available data are considered incomplete due to the reduced number of projectiles, targets, energies, angles, studied and limited accuracy of the setups.[56,57] Therefore, a source of uncertainties lies in the not well-known nuclear cross-sections.

The second source of discrepancies stems from uncertainties in the positioning of the mini-tracker in the experiment. The relatively short distance of 20.3 mm between the two sensitive layers, compared to the track length, induces a leverage effect. This effect can lead to significant variations in the position and orientation of the fragment tracks, even with small uncertainties in the mini-tracker positioning. This phenomenon is illustrated in Figure 4, which shows the distributions of the track angles relative to the beam axis. The spatial distribution of the detected fragments on the sensitive layers of the mini tracker, as seen in Figure 3, is intricately shaped by the detector geometry and incident angle of the fragment tracks. Consequently, the shift is also evident in Figure 3 due to the different fall-offs that extend towards the top edge of the detected fragments across the sensitive layer.

The simulated peak in Figure 4 exhibits an approximately 30% increase in fragment count compared to the measurements. Another geometric aspect, distinct from the detector's positioning that could explain these discrepancies pertains to the implementation of the HIT beam nozzle in FLUKA MC framework from HIT. Although the FLUKA MC framework accurately models the physical dose calculations, certain geometric approximations were introduced in the implementation of the HIT nozzle components.[21]

Examining the reconstructed fragment emission profiles in Figure 6, despite an overall similar shape, the simulated profile is shifted downstream of the beam axis relative to the measurement. Previous studies, including our group,[10] and others,[58,59] have reported significant fragment production at the entrance of irradiated objects. Consequently, the expected alignment of the rising edge of the measured emission profile with the front of the phantom supports the hypothesis that the observed shift is due to positioning uncertainty in the mini-tracker.

In the context of the InViMo clinical trial, several measures were taken to maximize the reproducibility and absolute accuracy of the positioning of the detection system for the study of anatomical inter-fractional changes. These measures included the design and study of a structural rigidity of the monitoring system, its mounting on fixed columns anchored to the concrete floor of the treatment room, and procedures to facilitate its correct positioning using the laser positioning system of the treatment room.

This study has shown that the uncertainty in the mini-tracker position is the dominant uncertainty when measuring the fragmentation emission profiles. Considering the overall good agreement of the characteristics between the simulation and the measurement, the presented simulation scheme can be used to investigate relative changes in the distribution of reconstructed fragmentation vertices caused by inter-fractional anatomical changes. In particular, parameters that can only be studied via simulation will become accessible for an in-depth investigation. For example, simulations allow for the study of fragment species and energy distribution, as well as their spatial distribution without the influence of scattering and absorption in the phantom.

5 | CONCLUSIONS

This study presents the implementation of a MC framework for evaluating the potential of secondary-ion-based monitoring of (CIRT).

It focuses on the modeling of a custom-designed mini-tracker as a detection system for tracking secondary ions in ion-beam therapy. The performance of the implementation is evaluated by a comparison of the simulation results with experimental data acquired at the Heidelberg Ion Beam Therapy Center in Germany. The mini-tracker is composed of four pixelized silicon radiation detectors Timepix3 developed at CERN.

Our investigation reveals a robust agreement between experimental data and data obtained from the MC simulations, affirming the effective integration of the mini-tracker and the scoring mechanism within our FLUKA simulation framework. Uncertainties in the positioning of the tracking system were found to have a crucial impact on the results. Therefore, it is crucial to minimize them in future studies when comparing simulations with experimental data. Further improvements in the minor residual differences might be reached by a future reduction of the uncertainties in the modeling of nuclear fragmentation cross sections in FLUKA.

In this publication, we have demonstrated the accuracy of our simulation framework. We conclude that the framework is appropriate for the simulation of in-vivo monitoring of CIRT patients using secondary nuclear charged fragments.

ACKNOWLEDGMENTS

TG is funded by the Deutsche Forschungsgemeinschaft (DFG, German Research Foundation), Project No.: 426 970 603, and LK by the Nationales Centrum für Tumorerkrankungen (NCT, National Center for Tumor Diseases).

CONFLICT OF INTEREST STATEMENT

The authors declare no conflicts of interest.

ORCID

Pamela Ochoa-Parra
https://orcid.org/0009-0002-7373-7524

REFERENCES

1. Jäkel O. Physical advantages of particles: protons and light ions. *Br J Radiol*. 2020;93:20190428.
2. Yokoyama A, Kubota Y, Kawamura H, et al. Impact of interfractional anatomical changes on dose distributions in passive carbon-ion radiotherapy for prostate cancer: Comparison of vertical and horizontal fields. *Front Oncol*. 2020;10:1264.
3. Houweling AC, Fukata K, Kubota Y, et al. The impact of interfractional anatomical changes on the accumulated dose in carbon ion therapy of pancreatic cancer patients. *Radiother Oncol*. 2016;119:319-325.
4. Muraro S, Battistoni G, Collamati F, et al. Monitoring of hadrontherapy treatments by means of charged particle detection. *Front Oncol*. 2016;6:177.
5. Gwosch K, Hartmann B, Jakubek J, et al. Non-invasive monitoring of therapeutic carbon ion beams in a homogeneous phantom by tracking of secondary ions. *Phys Med Biol*. 2013;58:3755-3773.
6. Olsansky V, Granja C, Oancea C, et al. Spectral-sensitive proton radiography of thin samples with the pixel detector Timepix3. *J Instrum*. 2022;17:C04016.
7. Granja C, Oancea C, Jakubek J, et al. Wide-range tracking and LET-spectra of energetic light and heavy charged particles. *Nucl Instrum Methods Phys Res, Sect A*. 2021;988:164901.
8. Granja C, Uhlar R, Chuprakov I, et al. Detection of fast neutrons with the pixel detector Timepix3. *J Instrum*. 2023;18:P01003.
9. Fálix-Bautista R, Ghesquière-Diárickx L, Marek L, et al. Quality assurance method for monitoring of lateral pencil beam positions in scanned carbon-ion radiotherapy using tracking of secondary ions. *Med Phys*. 2021;48:4411-4424.
10. Ghesquière-Diérickx L, Schlechter A, Fálix-Bautista R, et al. Investigation of Suitable Detection Angles for Carbon-Ion Radiotherapy Monitoring in Depth by Means of Secondary-Ion Tracking. *Front Oncol*. 2021;11:780221.
11. Ghesquière-Diérickx L, Félix-Bautista R, Schlechter A, et al. Detecting perturbations of a radiation field inside a head-sized phantom exposed to therapeutic carbon-ion beams through charged-fragment tracking. *Med Phys*. 2022;49:1776-1792.
12. *Preliminary AdvaPIX TPX3 Quad Datasheet* for ADVACAM s.r.o.; 2022.
13. Kelleter L, Schmidt S, Subramanian M, et al. Characterisation of a customised 4-chip Timepix3 module for charged-particle tracking. *Radiat Meas*. 2024;173:107086.
14. Kelleter L, Marek L, Echner G, et al. An in-vivo treatment monitoring system for ion-beam radiotherapy based on 28 Timepix3 detectors. *Sci Rep*. 2024;14(1):15452.
15. Ferrari A, Sala P, Fasso A, Ranft J. FLUKA: A multi-particle transport code Technical Report CERN-2005-10, INFN/TC 05/11, SLAC-R-773. *CERN, INFN, SLAC*. October 12 2005.
16. Böhlen T, Cerutti F, Chin M, et al. The FLUKA Code: Developments and Challenges for High Energy and Medical Applications. *Nucl Data Sheets*. 2014;120:211-214.
17. Augusto R, Bauer J, Bouhali O, et al. An overview of recent developments in FLUKA PET tools. *Physica Med*. 2018;54:189-199.
18. Battistoni G, Bauer J, Boehlen TT, et al. The FLUKA Code: An Accurate Simulation Tool for Particle Therapy. *Front Oncol*. 2016;6:116.
19. Kozlowska WS, Böhlen TT, Cuccagna C, et al. FLUKA particle therapy tool for Monte Carlo independent calculation of scanned proton and carbon ion beam therapy. *Phys Med Biol*. 2019;64(7):075012.
20. Dedes G, Parodi K. Monte Carlo simulations of particle interactions with tissue in carbon ion therapy. *Int J of Part Ther*. 2016;2:447-458.
21. Parodi K, Mairani A, Brons S, et al. Monte Carlo simulations to support start-up and treatment planning of scanned proton and carbon ion therapy at a synchrotron-based facility. *Phys Med Biol*. 2012;57:3759-3784.
22. Mirandola A, Molinelli S, Vilches Freixas G, et al. Dosimetric commissioning and quality assurance of scanned ion beams at the Italian National Center for Oncological Hadrontherapy. *Med Phys*. 2015;42:5287-5300.
23. Schwaab J, Brons S, Fieres J, Parodi K. Experimental characterization of lateral profiles of scanned proton and carbon ion pencil beams for improved beam models in ion therapy treatment planning. *Phys Med Biol*. 2011;56:7813-7827.
24. RaySearch Laboratories.Accessed in January 2024. https://www.raysearchlabs.com
25. Lysakovski P, Kopp B, Tessonnier T, et al. Development and validation of MonteRay, a fast Monte Carlo dose engine for carbon ion beam radiotherapy. *Med Phys*. 2024;51(2):1433-1449.
26. Battistoni G, Cerutti F, Fassò A, et al. The FLUKA code: description and benchmarking. *AIP Conf Proc*. 2007;896:31-49.
27. Böhlen TT, Cerutti F, Dosanjh M, et al. Benchmarking nuclear models of FLUKA and GEANT4 for carbon ion therapy. *Phys Med Biol*. 2010;55:5833-5847.
28. Mairani A, Brons S, Cerutti F, et al. The FLUKA Monte Carlo code coupled with the local effect model for biological calculations in carbon ion therapy. *Phys Med Biol*. 2010;55:4273-4289.
29. Kox S, Gamp A, Cherkaoui R, et al. Direct measurements of heavy-ion total reaction cross sections at 30 and 83 MeV/nucleon. *Nucl Phys A*. 1984;420:162-172.
30. Kox S, Gamp A, Perrin C, et al. Trends of total reaction cross sections for heavy ion collisions in the intermediate energy range. *Phys Rev C*. 1987;35:1678-1691.
31. Fang DQ, Shen WQ, Feng J, et al. Measurements of total reaction cross sections for some light nuclei at intermediate energies. *Phys Rev C*. 2000;61:064311.
32. Sihver L, Tsao CH, Silberberg R, Kanai T, Barghouty AF. Total reaction and partial cross section calculations in proton-nucleus ($Z_t \leq 26$) and nucleus-nucleus reactions (Z_p and $Z_t \leq 26$). *Phys Rev C Nucl Phys*. 1993;47:1225-1236.
33. Zhang H, Shen W, Ren Z, et al. Measurement of reaction cross section for proton-rich nuclei (A < 30) at intermediate energies. *Nucl Phys A*. 2002;707:303-324.
34. Takechi M, Fukuda M, Mihara M, et al. Reaction cross sections at intermediate energies and Fermi-motion effect. *Phys Rev C*. 2009;79:061601.
35. Haettner E, Iwase H, Schardt D. Experimental fragmentation studies with 12C therapy beams. *Radiat Prot Dosim*. 2006;122:485-487.
36. Bauer J, Sommerer F, Mairani A, et al. Integration and evaluation of automated Monte Carlo simulations in the clinical practice of scanned proton and carbon ion beam therapy. *Phys Med Biol*. 2014;59(16):4635-4659.
37. Mein S, Kopp B, Tessonnier T, et al. Dosimetric validation of Monte Carlo and analytical dose engines with raster-scanning 1H, 4He, 12C, and 16O ion-beams using an anthropomorphic phantom. *Physica Med*. 2019;64:123-131.

38. Tessonnier T, Mairani A, Brons S, et al. Helium ions at the heidelberg ion beam therapy center: comparisons between FLUKA Monte Carlo code predictions and dosimetric measurements. *Phys Med Biol*. 2017;62:6784-6803.
39. Combs SE, Jäkel O, Haberer T, Debus J. Particle therapy at the Heidelberg Ion Therapy Center (HIT) – Integrated research-driven university-hospital-based radiation oncology service in Heidelberg, Germany. *Radiother Oncol*. 2010;95:41-44.
40. Haberer T, Becher W, Schardt D, Kraft G. Magnetic scanning system for heavy ion therapy. *Nucl Instrum Methods Phys Res, Sect A*. 1993;330:296-305.
41. Fassò A, Ferrari A, Ranft J, Sala P. FLUKA: Status and Prospective for Hadronic Applications. *Proc. MonteCarlo 2000 Conference*. 2001;2000:159-164.
42. Battistoni G, Cerutti F, Engel R, et al. Recent Developments in the FLUKA Nuclear Reaction Models. *Proc. 11th Int Conf Nucl React*. 2006:483-495.
43. Ferrari A, Ranft J, Roesler S, Sala P. Cascade particles, nuclear evaporation, and residual nuclei in high energy hadron-nucleus interactions. *Zeitschrift fü Physik C*. 1996;70:413-426.
44. Cavinato M, Fabrici E, Gadioli E, Gadioli Erba E, Galbiati E. Monte Carlo calculations using the Boltzmann Master Equation theory of nuclear reactions. *Phys Lett B*. 1996;382:1-5.
45. Cavinato M, Fabrici E, Gadioli E, Gadioli Erba E, Riva G. Monte Carlo calculations of heavy ion cross-sections based on the Boltzmann Master equation theory. *Nucl Phys A*. 2001;679:753-764.
46. Fassò A, Ferrari A, Ranft J, Sala P. FLUKA 2021.2 Release Notes. [Online]. Accessed September 16, 2024. http://www.fluka.org/fluka.php?id=release_notes&mm2=3
47. Fassò A, Ferrari A, Sala PR. Electron-Photon Transport in FLUKA: Status. In: Kling A, Barão FJC, Nakagawa M, Távora L, Vaz P, eds. *Adv Monte Carlo for Radiat Phy, Part Transp Simul Appl*. Springer Berlin Heidelberg; 2001:159-164.
48. Vähänen S. Solutions for Flip Chip Bonding of Future Pixel Detectors. In: *Proceedings of Science*, CERN; 2017, Presented at The 26th International Workshop on Vertex Detectors.
49. Henriquet P, Testa E, Chevallier M, et al. Interaction vertex imaging (IVI) for carbon ion therapy monitoring: a feasibility study. *Phys Med Biol*. 2012;57:4655-4669.
50. Cirrone P, Petringa G. *Monte Carlo in Heavy Charged Particle Therapy: New Challenges in Ion Therapy*. CRC Press; 2023.
51. Aricò G, Gehrke T, Gallas R, Mairani A, Jäkel O, Martišíková M. Investigation of single carbon ion fragmentation in water and PMMA for hadron therapy. *Phys Med Biol*. 2019;64(5):055018.
52. Schall I, Schardt D, Geissel H, et al. Charge-changing nuclear reactions of relativistic light-ion beams ($5 \leq Z \leq 10$) passing through thick absorbers. *Nucl Instrum Methods Phys Res, Sect B*. 1996;117:221-234.
53. Haettner E, Iwase H, Schardt D. Experimental fragmentation studies with 12C therapy beams. *Radiat Prot Dosim*. 2006;122:485-487.
54. Haettner E, Iwase H, Krämer M, Kraft G, Schardt D. Experimental study of nuclear fragmentation of 200 and 400 MeV/u (12)C ions in water for applications in particle therapy. *Phys Med Biol*. 2013;58:8265-8279.
55. Golovchenko A, Skvarč J, Yasuda N, et al. Total charge-changing and partial cross-section measurements in the reaction of 110MeV/u 12C with paraffin. *Radiat Meas*. 2001;34:297-300.
56. Durante M, Paganetti H. Nuclear physics in particle therapy: a review. *Rep Prog Phys*. 2016;79:096702.
57. Muraro S, Battistoni G, Kraan A. Challenges in Monte Carlo Simulations as Clinical and Research Tool in Particle Therapy: A Review. *Front Phys*. 2020;8:567800.
58. Rucinski A, Battistoni G, Collamati F, et al. Secondary radiation measurements for particle therapy applications: Charged particles produced by 4He and 12C ion beams in a PMMA target at large angle. *Phys Med Biol*. 2018;63:055018.
59. Bey A, Ma J, Furutani KM, et al. Nuclear Fragmentation Imaging for Carbon-Ion Radiation Therapy Monitoring: an In Silico Study. *Int J Part Ther*. 2021;8(4):25-36.

How to cite this article: Ochoa-Parra P, Schweins L, Abbani N, Ghesquière-Diérickx L, Gehrke T, Jakubek J, et al. Experimental validation of a FLUKA Monte Carlo simulation for carbon-ion radiotherapy monitoring via secondary ion tracking. *Med Phys*. 2024;51:9217–9229.
https://doi.org/10.1002/mp.17408